IEEE Access
Multidisciplinary | Rapid Review | Open Access Journal

Received July 29, 2021, accepted August 18, 2021, date of publication August 23, 2021, date of current version August 30, 2021.

Digital Object Identifier 10.1109/ACCESS.2021.3106735

Design of Conformal Spiral Dual-Band Antenna for Wireless Capsule System

KUO LIU[1,2], RUIPENG LIU[1,2], WENJIE CUI[1,2], (Student Member, IEEE), KANGLONG ZHANG[1,2], (Member, IEEE), MENGJUN WANG[1,2], CHAO FAN[1,2], HONGXING ZHENG[1,2], (Senior Member, IEEE), AND ERPING LI[1,3], (Fellow, IEEE)

[1]State Key Laboratory of Reliability and Intelligence of Electrical Equipment, Hebei University of Technology, Tianjin 300132, China
[2]School of Electronics and Information Engineering, Hebei University of Technology, Tianjin 300401, China
[3]University of Illinois at Urbana–Champaign Institute, Zhejiang University, Haining 314400, China

Corresponding author: Hongxing Zheng (hxzheng@hebut.edu.cn)

This work was supported by the National Natural Science Foundation of China under Grant 62071166 and Grant 62071424.

ABSTRACT This paper presents a conformal spiral antenna that is miniaturized and with dual-resonant for the wireless implantable capsule system. The spiral antenna conforms to a swallowable capsule with a radius of 3 mm and a length of 26 mm without occupying the internal space of the capsule. The compact antenna adopts two spiral arms to extend the effective current path for miniaturization. Biocompatible flexible polyimide was used as the dielectric substrate and capsule shell, achieving conformal properties of the antenna as well as compatibility with human tissue. The antenna has been simulated in different environmental models. The bandwidth of the antenna can reach 39.16 % (1.82 GHz-2.76 GHz) and 12.06 % (5.36 GHz-6.06 GHz) at 2.4 GHz and 5.8 GHz. The maximum gains of −35.2 dBi and −28.1 dBi can be achieved at 2.4 GHz and 5.8 GHz, respectively. In addition, the transmission characteristics of the antenna were experimentally verified in the minced pork and pig intestine. By analyzing the communication link, the communication distance between transceivers at 2.4 GHz and 5.8 GHz can meet 14 m and 5 m. These results show that the proposed antenna is suitable for wireless implantable capsule systems.

INDEX TERMS Implantable capsule system, conformal antenna, dual-resonant, spiral antenna.

I. INTRODUCTION

Nowadays, wireless technology is widely used in implantable medical devices as it gets rid of the body from the limitations of wired devices [1]. In recent years, implantable devices can be implanted into the human body for the auxiliary treatment of various diseases, including capsule endoscopes [2], cardiac pacemakers [3], and intracranial pressure monitoring [4].

A wireless implantable capsule system with dual-band wideband antennas is selected for transmission as capsule speculum and cardiac pacemaker, as showing in Fig. 1. The wireless implantable capsule is promising to be used in the digestive system as a capsule speculum, and the heart as a cardiac pacemaker as long as changing its internal structure. The operating band of the proposed antenna could cover 2.42-2.48 GHz and 5.725-5.850 GHz, both of which belong to the industrial, scientific, and medical (ISM) frequency bands [5].

The associate editor coordinating the review of this manuscript and approving it for publication was Debdeep Sarkar.

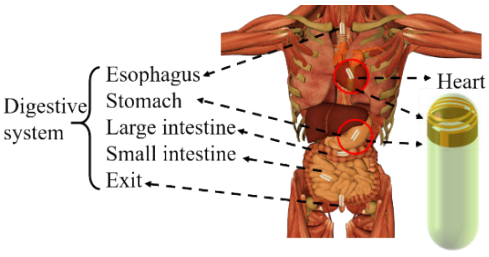

FIGURE 1. Wireless implantable capsule system works in the body.

With the development of medical technology, the demand for the transmission of real-time video is greater than for the transmission of simple pictures [6]. The transmission antenna with a wideband should be designed to meet the transmission needs of the implantable capsule system to be able to transmit video and other big data signals in real-time. In addition, to adapt to the complex implanted environment and improve the robustness of the antenna, it is required that the implanted antenna should be achieved

a wideband [7]. Due to the requirements for high data transfer rates, the life cycle of the implanted system needs to be as long as possible [8]. To extend the battery life, the antenna can be made with dual-frequency or multi-frequency [9]. Features, so that the system has dual-mode working characteristics. Therefore, designing a dual-frequency and broadband implanted antenna has important research value and significance. In [10], a spiral patch, high-dielectric substrate, and an open-end ground slot were used to achieve the multi-frequency at 402 MHz, 1.6GHz, and 2.4 GHz, and the maximum bandwidth of 219 MHz is obtained. Although this design implements multi-frequency features, the bandwidth is relatively small and takes up some space for implantable devices. In [11], the proposed antenna is designed to operate in 915 MHz and 2.45 GHz with the bandwidth of 107.5 MHz and 560 MHz, by adding an open-ended ground slot, shorting pin, and hexagonal and T-shaped slots in the radiator. Though its bandwidth can be increased, its complex structure increases the dimensions of the device. In studies [12], [13], although dual-band or multi-band characteristics are realized, the problems of narrow bandwidth and large internal space occupied still exist. Due to the limitations of space in implantable devices, how to maintain antenna dual-band and broadband while reducing the space occupied by the antenna is the top priority. Some miniaturization techniques, such as high dielectric constant substrate [14], [15], meandered line [16], spiral line [10], opening slot [17], and adding shorting pins [18], as well as stacked antennas [19], are used to reduce the space. However, these miniaturization technologies usually bring difficulties to the antenna design and production process and still occupy the limited space. Compared with the use of miniaturization, conformal can improve miniaturization performance. The conformal structure can effectively use the surface of the capsule, to avoid competing with the electronic components inside the capsule for the valuable space of capsules [20], [21]. The conformal characteristics are achieved by using flexible materials for bending, such as in studies [22], although the proposed antennas can be conformal with flexible materials, their performance fails to achieve multi-band and wide-band. Based on the above literature considerations, how to design a conformal antenna that has wide dual-band characteristics and reduces the contact area with the internal circuit is a problem worthy of consideration.

In this approach, a dual-band spiral antenna is investigated. It is conformed to a wireless implantable capsule system with the size of $\pi \times 3^2 \times 26$ mm^3. We implanted the antenna in the large intestine model and heart simulation model to verify the stability. To ensure safety, the specific absorption rate (SAR) has been analyzed. The entire system is also conducted in the different aforementioned heterogeneous implanted organs. A lot of experiments have been verified our design. Minced pork and pig intestine are used as the measured materials environment to the simulated human body. A significant result has been obtained.

II. DESIGN AND ANALYSIS OF ANTENNA

A. THE STRUCTURE OF THE ANTENNA

The implantable antenna works inside the body; and the size must be small enough, without affecting the surrounding tissues. The conformal structure is one of the best for the antennas which takes up almost no space [23]. The antenna proposed in this work uses a conformal design of the spiral structure and the hemispherical structure of the capsule. The structure of the antenna is mainly made up of two spiral arms. One arm is composed of a rectangular patch surrounding a hemispherical function. Another is obtained by rotating the first arm 180 degrees around the center. The hemispherical parameter function is as follows

$$x_t = \sqrt{r^2 - (S \times t/2\pi)^2} \times \sin t \quad (1)$$

$$y_t = \sqrt{r^2 - (S \times t/2\pi)^2} \times \sin t \quad (2)$$

$$z_t = S \times t/2\pi \quad (3)$$

In the above function, t is a variable, the range of t is 0-$n \times 2\pi$, n is the number of turns of the spiral, r is the radius of the hemispherical spiral, and S is the pitch. The x_t is the position coordinate function in the x-direction of the variable t, the y_t is the position coordinate function in the y-direction of the variable t and the z_t is the position coordinate function in the z-direction of the variable t. As illustrated in Fig. 2(a), the two spiral arms relate to two strip lines and are distributed on both sides of the annular dielectric substrate under the spiral arms.

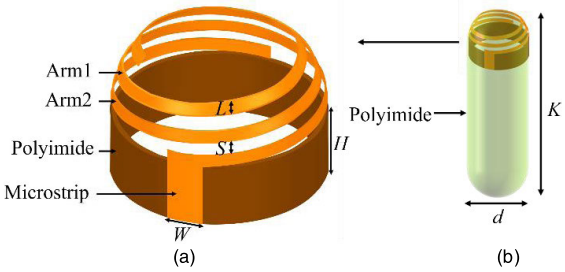

FIGURE 2. Structure of antenna and wireless implantable capsule, (a) antenna (b) wireless implantable capsule.

The dielectric is polyimide with 0.15 mm thickness which has a relative permittivity ε_r of 3.5, loss tangent tanδ of 0.008. The antenna is installed inside the top of the capsule with a length of K and a diameter of d at both ends of the sphere. The thickness of the outer layer of the capsule is 0.15 mm thick.

B. THE SIMULATION ENVIRONMENT

The wavelength in the human body is shorter than in the free space due to the antenna is affected by the relatively high permittivity of the human tissue, which works to profitably miniaturize the physical size of the antenna [24]. A simple muscle model, a large intestine model, and a heart model were established to simulate different working environments.

Electromagnetic properties of human tissues in various parts are tabulated in Table 1 [25].

TABLE 1. Dielectric properties of biological tissues at 2.4 GHz and 5.8 GHz.

Tissue type	2.4GHz		5.8GHz	
	ε_r	δ(S/m)	ε_r	δ(S/m)
Muscle	52.791	1.705	48.485	4.962
Fat	5.285	0.102	4.955	0.293
Mucous Membrane	42.923	1.5618	38.624	4.342

C. PARAMETER STUDY AND DISCUSSION

We implant the antenna in the single muscle simulation model which dimension is $\pi \times 50^2 \times 100$ mm^3 as shown in Fig. 3. According to the effective current distribution at 2.4 GHz and 5.8 GHz of the antenna in Fig. 4, we can see that different parts of the antenna excite the resonance at different frequencies. We analyze some important antenna structural parameters. Firstly, the antenna mainly depends on the spiral arm radiation, so the spiral arm around the number of turns parameter n and the winding line width L of the spiral arm have a great impact on the performance of the antenna. $|S_{11}|$ with different numbers of turns n and the winding line width L are presented in Fig. 5.

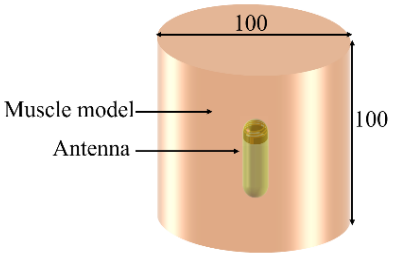

FIGURE 3. Antenna working in the single muscle simulation model.

It is observed that as the turns of the spiral arm changed, the effective path of the current increased, and the whole operating frequency moved with n changing from 0.85 to 1.6, as shown in Fig. 5 (a). The $|S_{11}|$ with different L is presented in Fig. 5 (b). It is observed the higher frequency point decrease and bandwidth in the low band increases as the winding line width L increases, which means that the change of L has a more obvious impact on the high frequency. According to the above results, the optimal n is 1.35, and the optimal size L is 0.5 mm.

In addition to the spiral arm, we have studied the influence of the size of the ground plane and the width of the antenna's microstrip. The $|S_{11}|$ with different heights of the ground H is shown in Fig. 6 (a). The $|S_{11}|$ with different widths of the antenna's microstrip W is shown in Fig. 6(b). The $|S_{11}|$ has not changed much when change the H and W, which means that the antenna is stable.

The parameter n affects the bandwidth at 2.4 GHz, and L affects the frequency at 5.8 GHz as shown in Fig. 5.

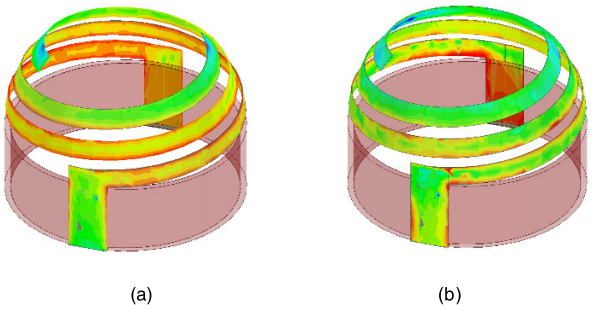

FIGURE 4. The effective current distribution of the antenna at (a) 2.4 GHz, and (b) 5.8 GHz.

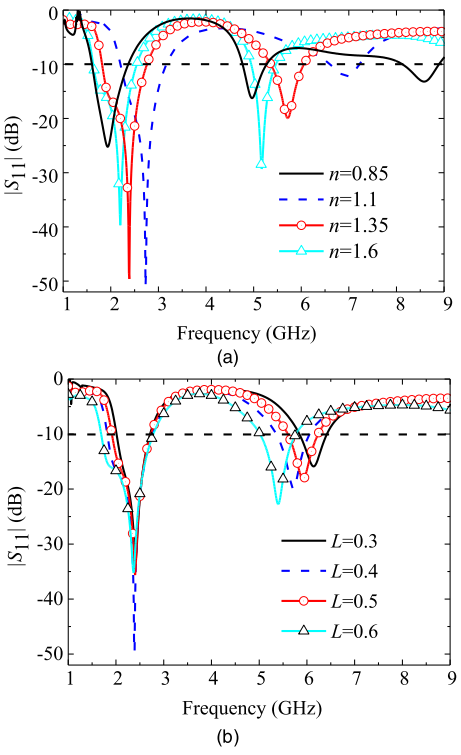

FIGURE 5. Simulated $|S_{11}|$ with different the number of turns n and winding line width of the spiral arm L, (a) is n with different size, and (b) is L with different size.

We studied the influence of the parameter n on the gain at 2.4 GHz and the influence of parameter L on the gain at 5.8 GHz as shown in Fig. 7. The parameter n and L affects both bandwidth and gains at 2.4 GHz and 5.8 GHz.

According to the above results, the optimal size of the antenna is tabulated in Table 2.

TABLE 2. Dimensions of the proposed system (unit: mm).

Dimensions	n	S	L	H	W	d	K
Size	1.35	1.45	0.5	1.8	1	6	26

D. SIMULATION WITH COMPLEX HUMAN MODEL

After analyzing the parameters of the antenna, the antenna was placed in a more complex simulation environment

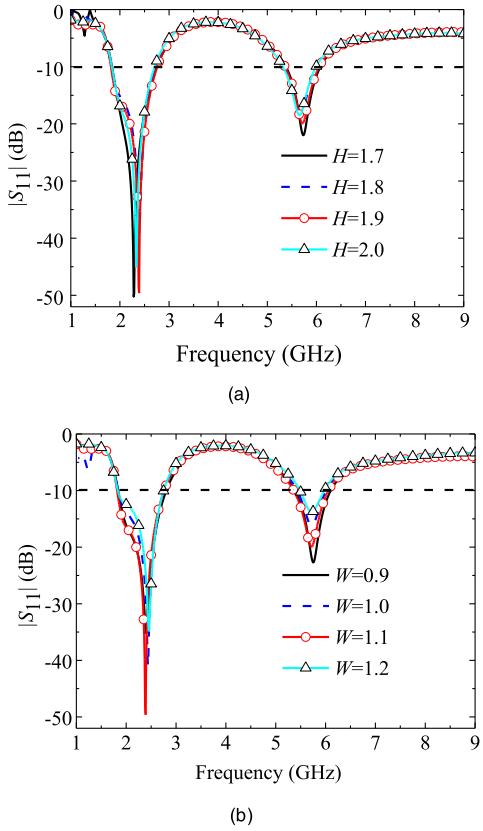

FIGURE 6. Simulated $|S_{11}|$ with different the height of the ground H and the width of the antenna's microstrip W, (a) is H with different size, and (b) is W with different size.

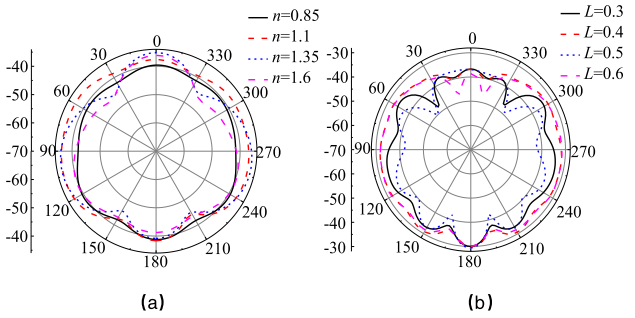

FIGURE 7. The influence of the parameters on the gain, (a) is the influence of the parameter n on the gain at 2.4 GHz, and (b) is the influence of the parameter L on the gain at 5.8 GHz.

to simulate to further verify the stability of the antenna performance. The large intestine model and heart model were established to simulate the working environment. The large intestine model is fat, muscle, and mucosa membrane from the outermost layer to the innermost layer. The thickness of this fat, muscle, and mucosa membrane is 15 mm, 20 mm, and 30 mm, respectively. The simulation model is a cylinder with a height of 100 mm, as shown in Fig. 8. And then, we established the heart model with fat, outer mucosa membrane, muscle, and mucosa membrane from the outermost layer to the innermost layer. The thickness of this fat, second layer

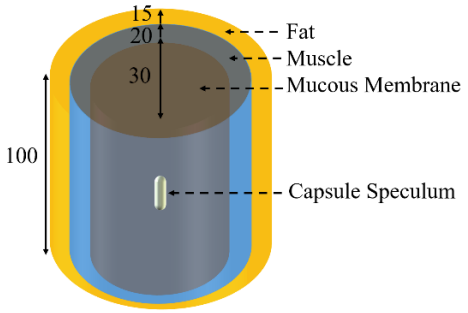

FIGURE 8. The environment of the proposed system is a capsule speculum working in the large intestine model.

mucosal membrane, muscle, and internal mucosa membrane is 10 mm, 5 mm, 10 mm, and 35 mm. The model is a sphere with a radius of 60 mm, as shown in Fig. 9. Then we compared the $|S_{11}|$ in a complex and simple environment as shown in Fig. 10. According to the results, the proposed antenna could work stably in different environments due to the stability of the antenna structure and the protective effect of the capsule shell.

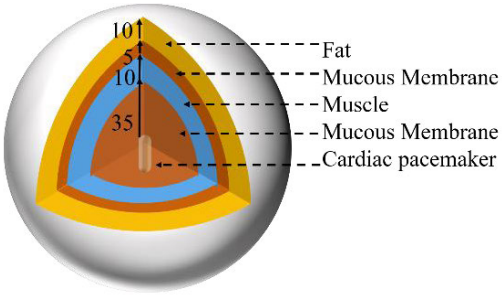

FIGURE 9. The environment of the proposed system as a cardiac pacemaker working in the heart model.

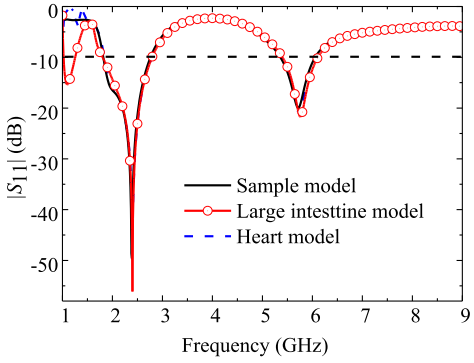

FIGURE 10. Simulation of antenna $|S_{11}|$ in different environments.

III. RADIATION PERFORMANCE EVALUATION

A. RADIATION PERFORMANCE AT DIFFERENT ORIENTATIONS

When the antenna enters the human digestive tract, its position and orientation will be changed. We study the radiation

pattern in different orientations 0, 45, and 90 degree-directed as shown in Fig. 11. The radiation patterns at 2.4 GHz are shown in Fig. 12. By increasing the direction angle, the antenna radiation pattern is changed. The gains at 2.4 GHz are −35.2 dBi, −35.0 dBi and −35.0 dBi at orientations 0, 45 and 90 degree-directed, respectively. The gains at 5.8 GHz are −28.1 dBi, −27.6 dBi and −25.9 dBi at orientations 0, 45 and 90 degree-directed, as shown in the Fig. 13. And the peak radiation efficiencies at 2.4 GHz and 5.8 GHz are 1.23 % and 1.47 %, respectively. So high-quality performance of the antenna can be ensured at different capsule orientations inside the body.

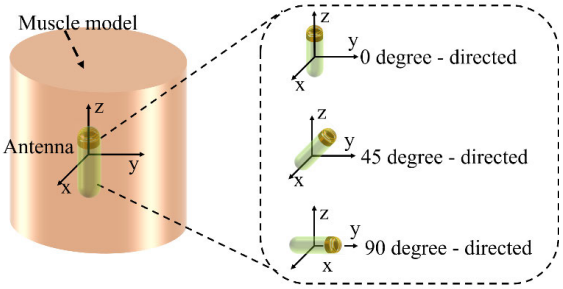

FIGURE 11. The system is inserted inside the model with three typical orientations of 0 degree, 45 degree, and 90 degree-directions.

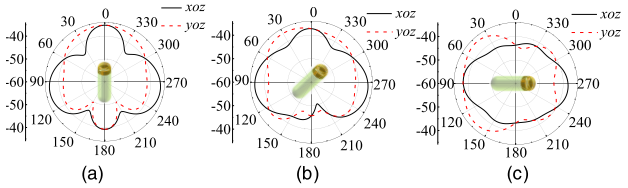

FIGURE 12. Simulated 2D far-field patterns with three typical implant orientations at 2.4GHz, (a) is 0 degree, (b) is 45 degree-directions, (c) is 90 degree-directions.

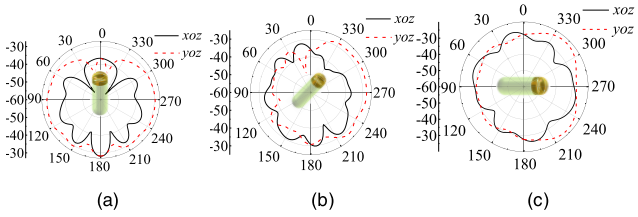

FIGURE 13. Simulated 2D far-field patterns with three typical implant orientations at 5.8 GHz, (a) is 0 degree, (b) is 45 degree-directions, (c) is 90 degree-directions.

B. THE SAR OF SYSTEM

The safety problem of the implantable antenna should be considered, where the specific absorption rate (SAR) is usually regarded as the evaluation standard for the implantable antenna, that the SAR levels averaged over 1-g of human tissue should be less than 1.6 W/kg [25]. Fig.14 displays the SAR of the antenna in different simulation models at 2.4 GHz.

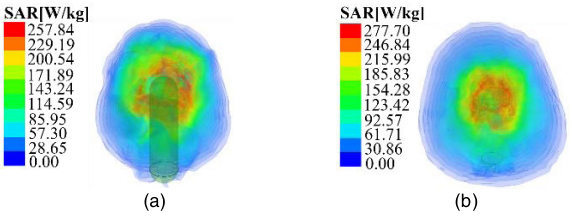

FIGURE 14. SAR of the antenna in the simulation model at 2.4 GHz, (a) in the large intestine simulated model, (b) in the heart simulated model.

Fig. 15 displays the SAR of the antenna in different simulation models at 5.8 GHz. The simulation models are the large intestine and heart simulated models as shown in Fig. 8 and Fig. 9. The maximum averaged SAR in 1-g of the large intestine and the heart at 2.4 GHz and 5.8 GHz are listed in Table 3 when the input power is 1W. According to the results, we can calculate the maximum input power of the antenna in the large intestine simulation model and heart simulated model at 2.4 GHz and 5.8 GHz when the SAR of the antenna is less than 1.6 W/kg. The SAR and the max allowed input power are listed in Table 3.

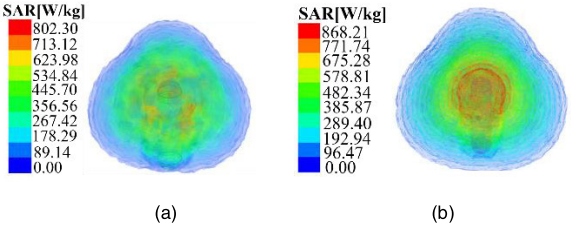

FIGURE 15. SAR of the antenna in the simulation model at 5.8 GHz, (a) in the large intestine simulated model, (b) in the heart simulated model.

TABLE 3. Maximum SAR values (input power = 1 W) and allowed input power for the antenna in the large intestine and heart.

Frequency	Maximum SAR(W/kg)		Maximum allowed power (mW)	
	large intestine	heart	large intestine	heart
2.4 GHz	257.8	277.7	6.22	5.75
5.8 GHz	802.3	868.2	1.99	1.82

The comparison with the proposed antennas in the previous work is displayed in Table 4. Compared with other dual-band or multi-band antennas, the proposed antenna achieved wide dual-band and conformality.

IV. MEASUREMENT RESULTS ANALYSIS

Fig 16 is the antenna designed according to Table 2, measured in minced pork and pig intestine. The antenna is composed of a radiating patch wrapped around the capsule shell to verify the performance of the designed antenna structure.

Fig. 17 is the simulated and measured $|S_{11}|$ of the antenna in minced pork and pig intestine, and the result shows the bandwidth of the antenna could cover 2.42-2.48GHz and

TABLE 4. Compared of the proposed antenna with prior work.

Ref.	Frequency (MHz)	BW (MHz)	Gain (dBi)	SAR (W/kg)	Conformal
[2]	402	110.6(27.5%)	-30.8	289.0	Yes
	915	120.8(13.2%)	-19.7	263.5	
	1200	64.8(5.4%)	-18.7	214.9	
[6]	1420	1398-1431(2.4%)	-13.5	-	No
	2400	2370-2510(5.8%)	-11.3	-	
[10]	402	356-504(36.8%)	-30.5	588	No
	1600	1520-1693(10.8%)	-22.6	441	
	2450	2316-2529(8.7%)	-18.2	305	
[11]	915	107.5(11.7%)	-27.65	730.07	No
	2450	560(22.9%)	-22.99	591.40	
[12]	404	402-405(0.74%)	-3	-	No
	1413.5	1395-1432(3.3%)	-8	-	
[13]	403	393-440(11.7%)	-29.7	216.6	Yes
	915	888-973(9.3%)	-24.9	92.4	
	2450	2213-2700(19.9%)	-18.2	98.5	
[15]	902	800-1000(22.2%)	-26.71	-	No
	2400	2200-2630(17.9%)	-17.5	-	
This work	2400	1820-2760(39.2%)	-35.2	258.84	Yes
	5800	5360-6060(12.1%)	-28.1	802.30	

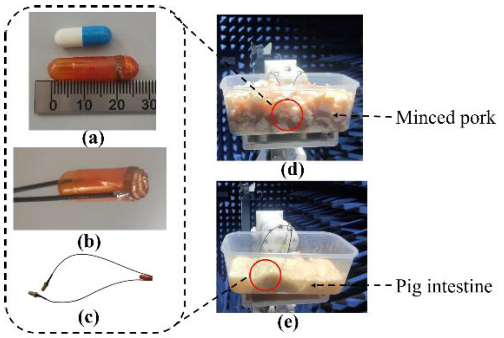

FIGURE 16. Photographs of the proposed double-arm helical antenna and the test of the antenna in minced pork and pig intestine. (a) comparison of antennas and ordinary medical capsules (b) the overall structure of the antenna(c) test of putting the antenna in minced pork and (d) in pig intestine.

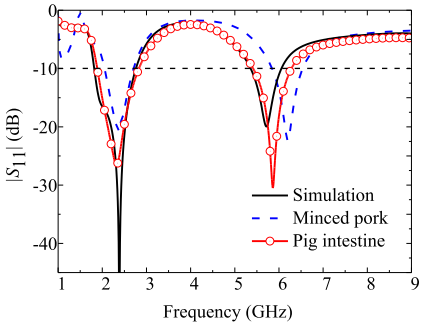

FIGURE 17. Simulated and measured $|S_{11}|$ of proposed antenna in minced pork and pig intestine.

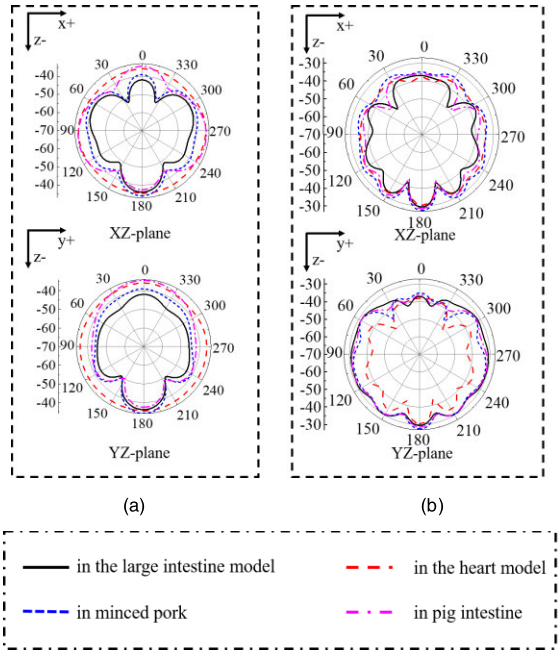

FIGURE 18. Comparison of the simulated and measured far-field radiation gain patterns. (a) 2.4 GHz. (b) 5.8 GHz.

5.725-5.850 GHz in different environments. Fig. 18 compares the simulated radiation patterns in the large intestine model and heart model and measured radiation patterns. Fig. 18(a) and Fig. 18(b) show the comparison of the simulation results and actual measurement of radiation pattern when the antenna at 2.4 GHz and 5.8 GHz. According to the compare results, the antenna has good radiation characteristics in the simulation and measurement environment.

V. LINK BUDGET ANALYSIS

Since different tissues and organs in the human body have their electrical characteristics, their coal-consuming characteristics will absorb electromagnetic waves. Energy, internal and external objects will reflect, diffract, scatter, and absorb electromagnetic fields to varying degrees, so the communication channel between the implanted antenna and the external device will be more complicated. To prove that the designed antenna can work normally and measure the effective communication distance of the implanted antenna in actual work, it is necessary to analyze the communication link. To simplify the calculation and make a preliminary assessment of the communication performance of the implantable antenna, we simply set the external channel environment as a free-space propagation model, with dB as the unit, the formula of path loss L_f is as follow [26]

$$L_f = 20\log_{10}(4\pi d/\lambda) \tag{4}$$

where d is the distance between the transmitting and receiving antennas, and λ is the free-space working wavelength. Link margin (*LM*) with the change of communication distance is used to measure the communication performance of the implanted antenna. The expressions related to the link margin are as follows [26]

$$LM = CNR_{link} - CNR_{required} \tag{5}$$

TABLE 5. Communication link budget-related parameters.

transmitter		
Operating frequency (GHz)	2.4 GHz	5.8 GHz
Tx power P_t (dBm)	7.60	2.60
Tx antenna Gain G_t (dBi)	-34.0	-40.4
Receiver		
Rx antenna Gain G_r (dBi)	2.15	2.15
Polarization	CP	CP
Ambient temperature T_0 (K)	293	293
Receiver Noise Figure NF (dB)	3.5	3.5
Boltzmann constant k	1.38×10^{-23}	1.38×10^{-23}
Noise power density (dB/Hz)	-199.95	-199.95
Signal quality		
Bit rate B_r (Mb/s)	1	1
Bit error rate	1.0×10^{-5}	1.0×10^{-5}
E_b/N_0 (ideal-BPSK) (dB)	9.6	9.6
Coding gain G_c (dB)	0	0
Fixing deterioration G_d (dB)	2.5	2.5

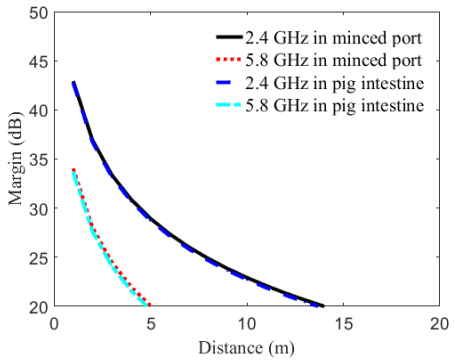

FIGURE 19. Link budget analysis at 2.4 GHz and 5.8 GHz when antenna works in minced port and pig intestine.

$$CNR_{link} = P_t + G_t - L_f + G_r - N_0 \quad (6)$$

$$CNR_{required} = E_b/N_0 + 10\log_{10} B_r - G_c + G_d \quad (7)$$

$$N_0 = 10\log_{10}(k) + 10\log_{10}(T_i) \quad (8)$$

$$T_i = T_0(NF - 1) \quad (9)$$

The CNR_{link} refers to the ratio of the signal power received by the external antenna at a certain distance and the noise power density when the implanted antenna is transmitted at a certain power. The $CNR_{required}$ refers to the carrier-to-noise ratio required by the receiving end to meet the requirements of a certain communication rate and bit error rate and is related to the sensitivity of the receiver. Here we adopt the BPSK modulation method, the bit error rate is required to be less than 1×10^{-5}, and the bit rate B_r is 1 Mb/s. Currently, the input power of the antenna working at 2.4 GHz and 5.8 GHz frequency is 7.60 dBm and 2.60 dBm, and the external receiving antenna adopts a circularly polarized antenna with a gain of 2.15 dBi. The above other values are listed in Table 5. The above formula can calculate the change of the communication link margin with the distance, as shown in Fig. 19. The transceiver distance reaches 14 m and 5 m when the communication link margin reached more than 20 dB at 2.4 GHz and 5.8 GHz.

VI. CONCLUSION

A spherical spiral structure and the conformal characteristics of the capsule shell are used to design a miniaturized implantable antenna that can be used as a capsule speculum and cardiac pacemaker. The Dual-band feature is implemented at 2.4 GHz and 5.8 GHz. In the simple muscle model established, the influence of the structure of the proposed antenna on the antenna is studied. The actual working environment of the antenna is simulated by building the large intestine model and heart model. The situation of different angular angles of the antenna in the process of the digestive tract system is also considered for simulation. Through the IEEE C95.1-1999 guidelines, the study of SAR ensures the safety of the proposed antenna to patients. Then compared with the previously proposed dual-band implanted antenna, the proposed antenna is distinct from the previously proposed antenna. We made a comparison of measured results in minced pork and pig intestines with the simulation to verify the feasibility of the antenna designed. Finally, by analyzing the communication link, the transceiver distance can reach 14 m and 5 m when the communication link margin reached more than 20 dB at 2.4 GHz and 5.8 GHz.

REFERENCES

[1] J. Shi, H. Liu, X. Wang, J. Zhang, F. Han, X. Tang, and J. Wang, "Miniaturized dual-resonant helix/spiral antenna system at MHz-band for FSK impulse radio intrabody communications," *IEEE Trans. Antennas Propag.*, vol. 68, no. 9, pp. 6566–6579, Sep. 2020.

[2] M. Yousaf, I. B. Mabrouk, F. Faisal, M. Zada, Z. Bashir, A. Akram, M. Nedil, and H. Yoo, "Compacted conformal implantable antenna with multitasking capabilities for ingestible capsule endoscope," *IEEE Access*, vol. 8, pp. 157617–157627, 2020.

[3] R. Liu, K. Zhang, Z. Li, W. Cui, W. Liang, M. Wang, C. Fan, H. Zheng, and E. Li, "A wideband circular polarization implantable antenna for health monitor microsystem," *IEEE Antennas Wireless Propag. Lett.*, vol. 20, no. 5, pp. 848–852, May 2021.

[4] M. Yousaf, I. B. Mabrouk, M. Zada, A. Akram, Y. Amin, M. Nedil, and H. Yoo, "An ultra-miniaturized antenna with ultra-wide bandwidth characteristics for medical implant systems," *IEEE Access*, vol. 9, pp. 40086–40097, 2021.

[5] F. Faisal, M. Zada, A. Ejaz, Y. Amin, S. Ullah, H. Yoo, K. N. Ketavath, D. Gopi, and S. S. Rani, "*In-vitro* test of miniaturized CPW-fed implantable conformal patch antenna at ISM band for biomedical applications," *IEEE Access*, vol. 7, pp. 43547–43554, 2019.

[6] R. B. Green, M. Hays, M. Mangino, and E. Topsakal, "An anatomical model for the simulation and development of subcutaneous implantable wireless devices," *IEEE Trans. Antennas Propag.*, vol. 68, no. 10, pp. 7170–7178, Oct. 2020.

[7] S. H. Lee, J. Lee, Y. J. Yoon, S. Park, C. Cheon, K. Kim, and S. Nam, "A wideband spiral antenna for ingestible capsule endoscope systems: Experimental results in a human phantom and a pig," *IEEE Trans. Biomed. Eng.*, vol. 58, no. 6, pp. 1734–1741, Jun. 2011.

[8] S. A. A. Shah and H. Yoo, "Radiative near-field wireless power transfer to scalp-implantable biotelemetric device," *IEEE Trans. Microw. Theory Techn.*, vol. 68, no. 7, pp. 2944–2953, Jul. 2020.

[9] T. Karacolak, A. Z. Hood, and E. Topsakal, "Design of a dual-band implantable antenna and development of skin mimicking gels for continuous glucose monitoring," *IEEE Trans. Microw. Theory Techn.*, vol. 56, no. 4, pp. 1001–1008, Apr. 2008.

[10] I. A. Shah, M. Zada, and H. Yoo, "Design and analysis of a compact-sized multiband spiral-shaped implantable antenna for scalp implantable and leadless pacemaker systems," *IEEE Trans. Antennas Propag.*, vol. 67, no. 6, pp. 4230–4234, Jun. 2019.
[11] F. Faisal, M. Zada, A. Ejaz, Y. Amin, S. Ullah, and H. Yoo, "A miniaturized dual-band implantable antenna system for medical applications," *IEEE Trans. Antennas Propag.*, vol. 68, no. 2, pp. 1161–1165, Feb. 2020.
[12] P. Soontornpipit and P. Satitvipawee, "Design and development of a dual-band PIFA antenna for wireless biotelemetry applications," in *Proc. Int. Electr. Eng. Congr. (iEECON)*, Mar. 2018, pp. 1–4.
[13] Z. Bao, Y.-X. Guo, and R. Mittra, "Single-layer dual-/tri-band inverted-f antennas for conformal capsule type of applications," *IEEE Trans. Antennas Propag.*, vol. 65, no. 12, pp. 7257–7265, Dec. 2017.
[14] W. Cui, R. Liu, L. Wang, M. Wang, H. Zheng, and E. Li, "Design of wideband implantable antenna for wireless capsule endoscope system," *IEEE Antennas Wireless Propag. Lett.*, vol. 18, no. 12, pp. 2706–2710, Dec. 2019.
[15] N. Pournoori, S. Ma, L. Sydanheimo, L. Ukkonen, T. Bjorninen, and Y. Rahmat-Samii, "Compact dual-band PIFA based on a slotted radiator for wireless biomedical implants," in *Proc. IEEE Int. Symp. Antennas Propag. USNC-URSI Radio Sci. Meeting*, Jul. 2019, pp. 13–14.
[16] H. Li, B. Wang, L. Guo, and J. Xiong, "Efficient and wideband implantable antenna based on magnetic structures," *IEEE Trans. Antennas Propag.*, vol. 67, no. 12, pp. 7242–7251, Dec. 2019.
[17] S. S. Md. Enan, A. Istiaque, and M. A. Hossain, "Design and characterization of miniaturized implantable PIFA antenna for MICS band application," in *Proc. IEEE Region Symp. (TENSYMP)*, Nov. 2020, pp. 254–257.
[18] A. Abdi, F. Ghorbani, H. Aliakbarian, T. K. Geok, S. K. A. Rahim, and P. J. Soh, "Electrically small spiral PIFA for deep implantable devices," *IEEE Access*, vol. 8, pp. 158459–158474, 2020.
[19] M. A. Elmansouri, E. A. Etellisi, and D. S. Filipovic, "Simultaneous transmit and receive spiral antenna with improved isolation," *IEEE Antennas Wireless Propag. Lett.*, vol. 19, no. 12, pp. 2145–2148, Dec. 2020.
[20] J. Yuan, K. Qiu, and Z. Chen, "A compact helix antenna with wide axial ratio bandwidth using a spiral microstrip coupling feedline for GNSS applications," *IEEE Antennas Wireless Propag. Lett.*, vol. 20, no. 4, pp. 433–437, Apr. 2021.
[21] A. Basir, M. Zada, Y. Cho, and H. Yoo, "A dual-circular-polarized endoscopic antenna with wideband characteristics and wireless biotelemetric link characterization," *IEEE Trans. Antennas Propag.*, vol. 68, no. 10, pp. 6953–6963, Oct. 2020.
[22] S. M. Asif, A. Iftikhar, B. D. Braaten, D. L. Ewert, and K. Maile, "A wideband tissue numerical model for deeply implantable antennas for RF-powered leadless pacemakers," *IEEE Access*, vol. 7, pp. 31031–31042, 2019.
[23] Z. Nie and Y. Yang, "A model independent scheme of adaptive focusing for wireless powering to in-body shifting medical device," *IEEE Trans. Antennas Propag.*, vol. 66, no. 3, pp. 1497–1506, Mar. 2018.
[24] A. Kiourti and K. S. Nikita, "A review of implantable patch antennas for biomedical telemetry: Challenges and solutions," *IEEE Antennas Propag. Mag.*, vol. 54, no. 3, pp. 210–228, Jun. 2012.
[25] *IEEE Standard for Safety Levels With Respect to Human Exposure to Radio Frequency Electromagnetic Fields, 3 kHz to 300 GHz*, Standard C95.1-1999, Apr. 1999.
[26] W. Xia, K. Saito, M. Takahashi, and K. Ito, "Performances of an implanted cavity slot antenna embedded in the human arm," *IEEE Trans. Antennas Propag.*, vol. 57, no. 4, pp. 894–899, Apr. 2009.

KUO LIU was born in Baoding, China, in 1998. He received the B.S. degree in communication engineering of electronics science and technology from Hebei University of Technology, Tianjin, China, in 2020, where he is currently pursuing the M.S. degree in electronics science and technology.

He has published four articles in refereed journals and conference proceedings. He held two Chinese patents issued in 2020. His current research interests include antennas and microwave circuits in wireless communication.

RUIPENG LIU was born in Luoyang, China, in 1994. He received the B.S. degree (Distinguished Engineer Class) in electronics engineering from Tianjin University of Technology and Education, Tianjin, China, in 2018. He is currently pursuing the M.S. degree in electronics science and technology with Hebei University of Technology, Tianjin.

He has published six articles in refereed journals and conference proceedings. He held four Chinese patents issued in 2019. His current research interests include antennas and computational electromagnetics.

WENJIE CUI (Student Member, IEEE) received the B.S. degree from Tianjin University of Technology and Education, Tianjin, China, in 2017. He is currently pursuing the Ph.D. degree with the School of Electronics and Information Engineering, Hebei University of Technology, Tianjin. His current interests include implantable antennas and devices, wireless power transfer, and wearable sensors and antennas.

He has published nine papers in refereed journals and conference proceedings. He has participated in the Chinese Graduate Mathematical Contest in Modeling and won the national third prize and second prize in 2017 and 2019, respectively.

KANGLONG ZHANG (Member, IEEE) received the B.E. degree in communication engineering from Zhengzhou University of Aeronautics, Zhengzhou, China, in 2016. He is currently pursuing the Ph.D. degree with the School of Electronics and Information Engineering, Hebei University of Technology, Tianjin, China.

He has published coauthored eight papers in refereed journals and conference proceedings. His research interests include antenna, microwave circuit, computational electromagnetics, and especially in the FDTD method.

MENGJUN WANG was born in Hebei, China, in 1978. He received the B.S. degree in information engineering and the M.S. degree in physical electronics from Hebei University of Technology, Tianjin, China, in 1999 and 2005, respectively, and the Ph.D. degree from Tianjin University, Tianjin, in 2008.

He is currently working as an Associate Professor with the School of Electronics and Information Engineering, Hebei University of Technology. His research interests include microwave radiofrequency technology, flexible electronic devices, and electromagnetic compatibility.

CHAO FAN was born in Hunan, China, in 1987. He received the Ph.D. degree in condensed matter physics from the Institute of Semiconductors, Chinese Academy of Sciences, Beijing, in 2015.

He is currently working as an Associate Professor with the School of Electronics and Information Engineering, Hebei University of Technology, Tianjin, China. He has more than 30 journal articles on the fields of low-dimensional electronic systems, opt-electron devices, and radiofrequency devices based on low-dimensional materials.

HONGXING ZHENG (Senior Member, IEEE) received the Ph.D. degree in electronic engineering from Xidian University, Xi'an, China, in 2002. He is currently a Professor with Hebei University of Technology, Tianjin, China. He has authored six books and book chapters and more than 200 journal articles and 100 conference papers. He holds 50 Chinese patents, issued in 2020. His current research interests include wireless communication, the design of microwave circuits and antennas, and computational electromagnetics.

He is also a Senior Member of the Chinese Institute of Electronics (CIE). He received the Young Scientists Award, in 2008, presented by the Tianjin Municipality, China.

ERPING LI (Fellow, IEEE) received the Ph.D. degree in electrical engineering from Sheffield Hallam University, Sheffield, U.K., in 1992. From 1993 to 1999, he was a Senior Research Fellow, the Principal Research Engineer, an Associate Professor, and the Technical Director at Singapore Research Institute and Industry. In 2000, he joined Singapore National Research Institute of High-Performance Computing as the Principal Scientist and the Director of the Department of the Electronic and Photonics. He also holds the post of a Distinguished Professor at Zhejiang University. He authored or coauthored more than 400 papers, published in various conference proceedings, and two books. His research interests include electrical modeling and design of micro/nano-scale integrated circuits, 3-D electronic package integration, and nano-plasmonic technology.

He is a fellow of the MIT Electromagnetics Academy, USA. He has received numerous awards including the IEEE Electromagnetic Compatibility (EMC) Richard Stoddard Award for Outstanding Performance. He has served as an Associate Editor for a number of IEEE TRANSACTIONS AND LETTERS. He has served as the general chair and the technical chair for many international conferences. He was the founding General Chair for the 2008, 2010, and 2012 Asia–Pacific EMC Symposium. He has been invited to give numerous invited talks and plenary speeches at various international conferences and forums.